Elastic anomalies associated with transformation sequences in perovskites: I. Strontium zirconate, $SrZrO_3$

2009 J. Phys.: Condens. Matter 21 015901

(http://iopscience.iop.org/0953-8984/21/1/015901)

J. Phys.: Condens. Matter **21** (2009) 015901 (14pp) doi:10.1088/0953-8984/21/1/015901

Elastic anomalies associated with transformation sequences in perovskites: I. Strontium zirconate, $SrZrO_3$

Ruth E A McKnight[1], C J Howard[1,2] and M A Carpenter[1]

[1] Department of Earth Sciences, University of Cambridge, Downing Street, Cambridge, CB2 3EQ, UK
[2] School of Engineering, University of Newcastle, Callaghan, NSW 2308, Australia

E-mail: ream3@cam.ac.uk

Received 22 August 2008, in final form 13 October 2008
Published 1 December 2008
Online at stacks.iop.org/JPhysCM/21/015901

Abstract

Elastic behaviour associated with the hierarchy of tilting transitions in $SrZrO_3$ has been examined using resonant ultrasound spectroscopy on a ceramic sample at temperatures between 153 and 1531 K. Changes in slope of the evolution of resonance frequencies with temperature indicate that phase transitions occur at 1038 K ($Pnma \leftrightarrow Imma$), 1122 K ($Imma \leftrightarrow I4/mcm$), and 1367 K ($I4/mcm \leftrightarrow Pm\bar{3}m$). Strain analysis of previously recorded neutron diffraction data shows that the $I4/mcm \leftrightarrow Pm\bar{3}m$ and $Pnma \leftrightarrow Imma$ transitions are close to tricritical in character, and that $Imma \leftrightarrow I4/mcm$ is first order. Deviations from the form of the elastic behaviour predicted by Landau theory are found. In particular, elastic softening in the vicinity of the $Imma \leftrightarrow I4/mcm$ transition suggests that local dynamical fluctuations between individual tilt systems occur, rather than a discontinuous switch from one phase to another. Determinations of the mechanical quality factor, Q, show that $SrZrO_3$ in the $Pm\bar{3}m$ phase is a classically high-Q (i.e. non-dissipating) cubic material. $I4/mcm$ and $Imma$ phases both have much greater dissipation (low Q), which is tentatively attributed to the mobility of twin walls. The room temperature $Pnma$ phase is unexpectedly much stiffer than both $I4/mcm$ and $Imma$ phases and has high Q. It appears that when two separate tilt systems operate, as in $Pnma$, they can interact to reduce strain/order parameter relaxations.

1. Introduction

Perovskite structures (ABO_3) are well known to undergo sequences of phase transitions due to structural distortions associated with changing temperature (Glazer 1972, 1975, Aleksandrov 1976, 1978, Salje 1989). Whether these transitions arise as a consequence of distortions of the BO_6 octahedral units, displacements of the B-cation within the octahedra, or tilting of the corner-linked BO_6 octahedra (Megaw 1973), they are commonly observed to give rise to large anomalies in elastic properties (e.g. Rehwald 1973, Lüthi and Rehwald 1981, Carpenter and Salje 1998, Harrison *et al* 2003, Carpenter 2006, Walsh *et al* 2008).

An example of a classically studied ferroelectric perovskite is $BaTiO_3$, in which transitions are associated with a single instability at the Γ-point of the Brillouin zone, where each Ti cation is displaced in a specified direction within its octahedron. The sequence of transitions for $BaTiO_3$, described in detail by Devonshire (1949, 1951, 1954), is cubic ↔ tetragonal ↔ orthorhombic ↔ rhombohedral. The transitions are at 400 K, 290 K and 190 K respectively and all phases are ferroelectric, except the cubic phase which is paraelectric (Schaller *et al* 2001). Sharp anomalies (minima) in the elastic modulus, E, associated with these transitions have been observed by Cheng *et al* (1994) by electrostatically driving the samples in flexural vibration. The same study also noted that each transition is accompanied by a narrow peak in the internal friction, Q^{-1}, as a function of temperature. Similar results for the tetragonal ↔ orthorhombic ↔ rhombohedral temperature region have been measured using an inverted torsion pendulum experiment by Zhang *et al* (1994). In principle, the different structures of $BaTiO_3$ occur in association with a single critical temperature but differ in the orientation of the order parameter. In terms of the three order parameter components aligned along

Table 1. Transition temperatures for $SrZrO_3$ from previous studies. $T1$ is the transition temperature for what we understand to be the $Pnma \leftrightarrow Imma$ transition, $T2$ is $Imma \leftrightarrow I4/mcm$, and $T3$ is $I4/mcm \leftrightarrow Pm\bar{3}m$. Transition temperatures presented in this study are added to the table for completion.

Paper	Method	Sample type	$T1$ (K)	$T2$ (K)	$T3$ (K)
Carlsson (1967)	Differential thermal analysis	Sintered pellet	1003 ± 25	1133 ± 25	
Carlsson (1967)	XRD	Sintered pellet	973	1103	1443
De Ligny and Richet (1996)	Drop calorimetry = heat capacity	Powder	995 ± 5	1105 ± 5	1440 ± 25
De Ligny and Richet (1996)	Energy dispersive XRD = thermal expansion	Powder	970		
Kennedy *et al* (1999)	Neutron diffraction and Rietveld refinement	Powder	1020		1360
Howard *et al* (2000)	High resolution neutron diffraction	Powder	1023 (contin.)	1113 (discont.)	1343 (contin.)
Matsuda *et al* (2003)	Differential scanning calorimetry	Sintered pellet	1041	1130	1376
Matsuda *et al* (2003)	Dilatometry = thermal expansion	Pellet	1035		
Fujimori *et al* (2004)	Raman spectroscopy	Solid (polymerized complex method)	995	1105	
This study	Resonant ultrasound spectroscopy	Sintered pellet	1038 ± 1	1122 ± 1	1367 ± 1

orthogonal axes, the tetragonal structure has $q_1 \neq 0, q_2 = q_3 = 0$, the orthorhombic structure has $q_1 = q_2 \neq 0, q_3 = 0$, and the rhombohedral structure has $q_1 = q_2 = q_3 \neq 0$. Devonshire (1949, 1951, 1954) showed that the full sequence should only be observed when the initial instability is first order in character (negative fourth order coefficient in a 246 Landau potential).

It is expected that exactly analogous sequences to that in $BaTiO_3$ should occur in structures where phase transitions are due to octahedral tilting rather than ferroelectric displacements. An R-point instability might give $Pm\bar{3}m \leftrightarrow I4/mcm$ ($q_1 \neq 0, q_2 = q_3 = 0$) $\leftrightarrow$ $Imma$ ($q_1 = q_2 \neq 0, q_3 = 0$) $\leftrightarrow$ $R\bar{3}c$ ($q_1 = q_2 = q_3 \neq 0$), for example. In addition, however, tilting transitions can be due to multiple instabilities with, in particular, simultaneous tilting associated with the special points M and R (Howard and Stokes 1998, Carpenter *et al* 2001, Carpenter 2007). The sequence of transitions in $SrZrO_3$ includes aspects of the hierarchy due to an R-point instability plus an M-point instability in the sequence, according to Howard *et al* (2000):

cubic ($Pm\bar{3}m$) $\overset{1343\text{ K}}{\longleftrightarrow}$ (cont.) tetragonal ($I4/mcm$, R only) $\overset{1113\text{ K}}{\longleftrightarrow}$ (discont.) pseudo-tetragonal ($Imma$, R only) $\overset{1023\text{ K}}{\longleftrightarrow}$ (cont.) ortho-rhombic. ($Pnma$, R and M)

A 246 Landau potential should, in principle, describe the structural sequence and order parameter evolution in $SrZrO_3$, in exactly the same manner as it does for $BaTiO_3$. The most stringent test of this is provided by analysis of elastic constants, which probe the second derivatives of free energy with respect to strain and are thus highly sensitive to the order parameter susceptibility. It has recently been found, however, that tilting transitions in $(Ca,Sr)TiO_3$ perovskites give rise to a complex pattern of elastic anomalies and acoustic dissipation, showing that the classical Landau description does not provide a complete description of real behaviour (Harrison *et al* 2003, Carpenter *et al* 2007, Walsh *et al* 2008). The question then arises as to whether deviations from classical behaviour are the same or different between transitions driven by octahedral tilting and ferroelectric displacements in perovskites.

The intrinsic physical properties of perovskites and the dynamic behaviour of their microstructures are important in a wide range of contexts, and both are strongly influenced by phase transitions. For example $(Mg,Fe)SiO_3$ perovskite forms a substantial proportion of the Earth's lower mantle, where it is believed to have $Pnma$ symmetry (Wentzcovitch *et al* 1993, Stixrude and Cohen 1993, Fiquet *et al* 1998, Ono *et al* 2004a); $CaSiO_3$ is present in the mantle in smaller proportions and may be cubic ($Pm\bar{3}m$) or tetragonal ($I4/mcm$) (Ono *et al* 2004b, Kurashina *et al* 2004, Caracas *et al* 2005, Jung and Oganov 2005, Li *et al* 2006a, 2006b, Adams and Oganov 2006). Confirmation of their presence depends on the velocities of seismic waves, which in turn depend on their elastic properties. In a completely different context, $Pnma$ manganite perovskites are also important for their remarkable electronic properties with the possibility of coupling between octahedral tilting and Jahn–Teller octahedral distortions (e.g. Goodenough 1998, Lufaso and Woodward 2004). In all these materials, the extent to which strain/order parameter coupling occurs has a strong bearing on the resulting elastic behaviour, and the mobility of transformation twin walls controls switching kinetics and acoustic dissipation.

Against this broader background, the present study is a detailed analysis of the elastic anomalies and acoustic dissipation which accompany octahedral tilting phase transitions in $SrZrO_3$. There have been many previous studies of this system and a summary of their suggested transition temperatures is given in table 1. The most recent high resolution powder neutron diffraction results of Howard *et al* (2000) are used here as a basis for interpreting the results of resonant ultrasound spectroscopy (RUS) measurements on a polycrystalline sample of $SrZrO_3$ over the temperature interval 153–1531 K. The paper is divided into several sections. Section 2 explains the way in which the experiments were carried out and results are presented in section 3. Section 4 presents an analysis of strain data across the transition sequence, section 5 contains a description of how the elastic properties are expected to behave according to Landau theory, and section 6 is a general discussion of

the elastic behaviour of the $SrZrO_3$ system as understood from the results of this study. In an accompanying paper (McKnight *et al* 2009), the elastic behaviour of ceramic samples of different compositions across the solid solution series with $SrZrO_3$ and $SrTiO_3$ end members is described.

2. Experimental details

2.1. Apparatus

The RUS system used for high temperature measurements consists of two alumina rods mounted horizontally inside a Netzsch 1600 °C furnace. The sample is prepared as a parallelepiped and is balanced across its corners between the ends of the rods inside the furnace. Piezoelectric transducers are attached to the other ends of the rods outside the furnace. One transducer acts as the driving resonator and the other as the detector using Dynamic Resonance System (DRS) M^3odulus II electronics. The low temperature system has the parallelepiped balanced directly between the two transducers, which are inserted vertically into a helium cryostat. These high temperature and low temperature RUS systems are described in detail by McKnight *et al* (2008, 2007), respectively. The only alteration to previously described experiments is that the low temperature transducer heads have been re-coated with gold, by vapour deposition, in order to reduce radio frequency interference.

2.2. Sample preparation and characterization

Strontium zirconate powder (<10 μm, Sigma-Aldrich) was ground in acetone in an agate ball-mill for 1 h at 600 rpm. Approximately 4 g of the milled powder was pressed into a pellet in a standard cylindrical IR pellet die (diameter 13 mm), using a bench-top press under ~4500 psi (≈31 MPa) of uniaxial pressure and under a vacuum generated by a rotary pump for approximately 5 min. The pellet was then annealed in air at 1600 °C for 48 h. Several parallelepipeds were cut from the pellet using a fine annular diamond saw, lubricated with paraffin. During the cutting process, the pellet was glued to a glass block using Crystalbond glue, manufactured by SPI supplies, with a softening temperature of 120–130 °C. Offcuts of the pellet were ground by hand in an acetone slurry, using an agate pestle and mortar, for characterization by powder x-ray diffraction. The room temperature diffraction pattern, collected with a Bruker D8 diffractometer using Cu Kα_1 radiation, contained only peaks which could be assigned to *Pnma* perovskite. SEM analysis in standard imaging modes of one of the pellet offcuts showed that individual grains were less than 10 μm across, with the smallest grain sizes at approximately 2 μm. Examination of a thin section of the same offcut under the petrographic microscope showed evidence of twins in some of the grains.

The parallelepiped selected for high and low temperature RUS experiments was examined under a binocular microscope to make sure that it was free from visible cracks. At room temperature, the dimensions of this sample were 1.861 mm × 2.922 mm × 4.699 mm, weight 0.1352 g, and density 5.2911 g cm^{-3}. This density is 97.2% of the theoretical density calculated from the lattice parameters given by Howard *et al* (2000) and the sample is therefore presumed to have ~2.8% porosity.

2.3. Data collection and analysis

Using the high temperature RUS system, the parallelepiped was heated from room temperature to 1531 in 30 K steps with a 15 min equilibration time at each temperature. It was then cooled back to room temperature in 10 K steps with a 10 min equilibration time. In the vicinity of the three known phase transition temperatures of $SrZrO_3$ (Howard *et al* 2000) the temperature increment was reduced to 1 K and the thermal equilibration time at each step was 5 min. The sample was then transferred to the low temperature RUS system where it was cooled from room temperature to 153 K in 40 K steps with equilibration at each temperature for 20 min. It was then heated back to room temperature in 5 K steps with 10 min equilibration at each step.

During heating and cooling, spectra were collected at each step after equilibration. For high temperature measurements, spectra were collected in the frequency range 200–1200 kHz with 50 000 data points. Low temperature measurements were taken in the range 200–1500 kHz, also with 50 000 data points. Room temperature spectra were collected before any high or low temperature experiments were carried out. These were taken in the frequency range 200–1200 kHz with the sample in four different orientations to ensure that all resonances of the sample were excited and observed.

All spectra were transferred to the software package Igor Pro (WaveMetrics) for detailed analysis. Peak positions and half-widths were determined for selected peaks by fitting with an asymmetric Lorentzian function, an approach analogous to that described by Schreuer *et al* (2003) and Schreuer and Thybaut (2005). The mechanical quality factor, Q, is given by $Q = f/\Delta f$, where f is the peak frequency and Δf is the peak width at half-maximum height. The inverse quality factor, Q^{-1}, is a measure of acoustic dissipation within the sample.

Bulk and shear moduli (K and G respectively) were determined by matching observed peak frequencies with calculated frequencies using the DRS software (Migliori and Sarrao 1997) and assuming an isotropic medium. The same sample dimensions and density were used for fits at all temperatures. No correction for thermal expansion was applied, due to the fact that the approximately linear thermal expansion of ~0.1% every 100 K seen in $SrZrO_3$ (Howard *et al* 2000, Matsuda *et al* 2003) will have negligible effects on values of K and G, and the general form of the elastic behaviour that is attributed to the effects of phase transitions will still be the same.

The relationship between the thermocouple reading and the actual temperature in the high temperature furnace was determined as part of this study, using known transition temperatures of single crystal quartz (846 K), $LaAlO_3$ (817 K) and $Ca_{0.7}Sr_{0.3}TiO_3$ (1204 K). It was found that a plot of the actual transition temperatures, T_{act}, against the observed transition temperatures, T_{obs}, for high temperature measurements, followed a straight line:

$$T_{act} = 4.3766 + 0.986\,04T_{obs}. \quad (1)$$

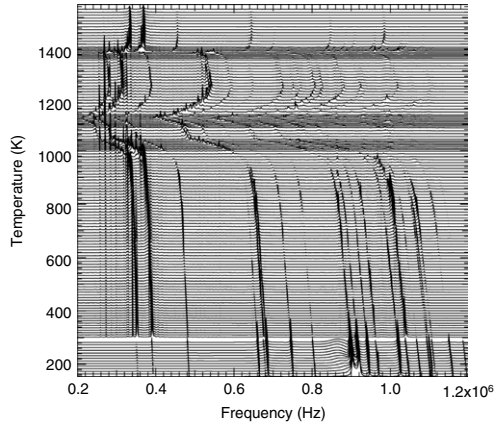

Figure 1. Stack of RUS spectra for $SrZrO_3$ collected in the frequency range 200–1200 kHz at temperatures between 153 and 1531 K. Above room temperature, spectra are those collected during cooling. Below room temperature, spectra collected during heating are shown. In this plot the y-axis is amplitude but the spectra have been displaced in proportion to the temperature at which they were collected. This temperature scale is then shown as the y-axis.

All temperatures quoted and used in the text and in figures throughout this paper have been corrected according to this calibration. No temperature corrections were carried out for measurements taken using the low temperature apparatus, as the known $Pm\bar{3}m \leftrightarrow I4/mcm$ transition in $SrTiO_3$ was observed exactly at 106 K, thus indicating that low temperature thermocouple readings are accurate to at least ± 1 K.

3. Results

3.1. Raw spectra

The influence of the three phase transitions of $SrZrO_3$ on its resonance peaks is immediately evident from the raw RUS spectra, shown stacked as a function of temperature in figure 1. Peaks in the spectra that are affected by temperature represent the vibrational frequencies of normal modes of the sample. Periodic, temperature-independent peaks at lower frequencies are due to resonances of the alumina rods and are referred to below as instrument noise.

The first thing that can be noticed about the sample resonances is that there are distinct changes in peak positions across the temperature range. In general, there is a steady but gentle decrease in peak frequency with increasing temperature across the whole range, presumably due to normal thermal elastic softening, however, substantial anomalies in this pattern are seen in the regions where transitions occur. On heating, the first transition is marked by significant softening (frequencies decrease rapidly) as it is approached from ∼950 K, with frequency evolution abruptly returning to the gentle decrease at 1038 K. The second transition is marked by the same pattern of softening below the transition, from ∼1090 K, which abruptly stops at 1122 K. Above this transition, however, there is significant stiffening (frequencies increase rapidly) for approximately 100 K. The third transition shows a similar pattern to the second, with the change in slope between softening and stiffening occurring at 1367 K. The temperature interval over which the effects of this phase transition are seen, however, is much smaller (only up to ∼20 K on either side of the minimum point).

The abrupt changes in slope of peak frequencies are believed to represent the temperatures at which the three phase transitions occur: $Pm\bar{3}m \leftrightarrow I4/mcm$ at 1367 K, $I4/mcm \leftrightarrow Imma$ at 1122 K, and $Imma \leftrightarrow Pnma$ at 1038 K. These temperatures are all only slightly higher than those quoted by Howard *et al* (2000) (1343 K, 1113 K and 1023 K respectively).

Additional features of the resonance peaks as they evolve with temperature are their changes in amplitude and width. At room temperature, all the peaks are sharp and strong. In the region of the three phase transitions, peaks are broad and have much smaller amplitudes, making it difficult to distinguish them from instrument noise in the most extreme cases. This is the case, especially at higher frequencies, for most peaks in spectra collected within the stability fields of the $Imma$ and $I4/mcm$ phases. In spectra from the cubic phase, peak resolution is much better again.

Finally, it is important to note that, although resonance peaks from the cubic phase are well resolved at first, their intensities decrease and their line widths increase at the highest temperatures. Above ∼1470 K, virtually all peaks in the spectra have disappeared.

3.2. Frequency, Q^{-1}, K and G variations

For ease of inspection, the measured peak frequencies of the first 3 peaks in the spectra are plotted across the full temperature range in figure 2(a). This clearly shows the changes in slope associated with each of the three phase transitions, with an overall gentle decrease as temperature increases across the entire range. Comparison of peak positions during heating and cooling runs (included for the third peak in figure 2(a)) shows that there is no obvious hysteresis in the phase transition temperatures. Resonance frequencies appear to be almost identical during heating and cooling, except at temperatures within the stability field of the $I4/mcm$ phase where peaks occur at significantly lower frequencies (up to 25 kHz) during heating than those recorded during cooling. This suggests some possible sensitivity to the twin configurations.

The full widths at half-maximum of the first three peaks were used to measure the quality factor, Q. The first 2 peaks in the spectra showed unreliable values for Q as they crossed many of the low frequency noise peaks. Peak overlap results in amplified peak amplitudes and therefore larger-than-expected peak widths and false values for Q. This amplification is rather useful, however, in that it allows the existence of low-Q peaks to be detected, even though absolute values of peak position and Q obtained from them are not accurate. The third peak has only a little overlap with noise peaks in spectra from the $I4/mcm$ and $Imma$ phases. Q^{-1} for the third peak, shown as a function of temperature in figure 2(b), therefore provides the best representation of acoustic dissipation in the sample.

Dissipation is very low and constant in the $Pnma$ phase ($Q^{-1} \approx 0.001$). This increases at around 950 K (the same

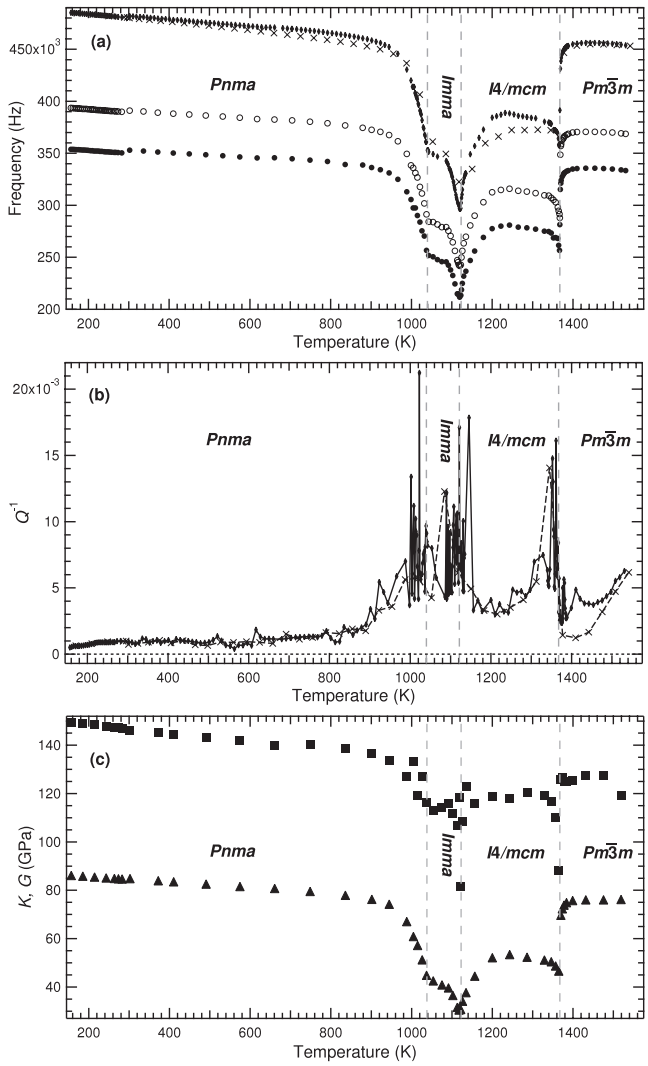

Figure 2. Analysis of RUS spectra of $SrZrO_3$ at temperatures between 153 and 1531 K. (a) shows measured frequencies for the first 3 peaks of the resonance spectra during heating for low temperature data and cooling for high temperature data (closed circles, open circles, and closed diamonds for the first, second and third peaks respectively). The frequencies of the third peak measured on cooling to low temperatures and heating to high temperatures are shown for comparison (crosses). (b) is the evolution of Q^{-1} for the third peak, measured on cooling from high temperatures and heating from low temperatures (closed diamonds connected with solid lines). Crosses connected with dashed lines represent the dissipation for heating above room temperature and cooling below room temperature. (c) shows the fitted values for bulk (K, squares) and shear (G, triangles) moduli based on peak positions measured during cooling from high temperatures and heating from low temperatures. Uncertainties in both K and G are within the bounds of the symbol sizes. The dashed vertical lines on all figures represent the phase transition temperatures estimated from the breaks in slope of peak frequencies.

temperature as the sudden decrease in frequencies) and stays at values of ∼0.004–0.007 throughout most of the stability fields of the $I4/mcm$ and $Imma$ phases. In the vicinity of each phase transition there are clear maxima in Q^{-1} of up to ∼0.02. The increase in Q^{-1} appears to start ∼50 K ahead of the presumed transition points, whether they are approached from above or below. During heating, Q^{-1} of the cubic phase at first reduces to values which are similar to those in the $Pnma$ stability field. On subsequent cooling, these remain slightly higher, however. Values for Q^{-1} in the $I4/mcm$, $Imma$ and $Pnma$ phases all seem to be similar during heating and cooling (figure 2(b)).

Fitted values for bulk and shear moduli (figure 2(c)) follow the same form as the frequency plot. These values are based on fits of approximately 20 resonance peaks for temperatures from room temperature up to 900 K. Between 900 K and 1365 K, only 5–10 peaks were measurable in the spectra and fits based on this number of resonances are less accurate. From 1365 K to 1475 K, fits are again based on ∼20 peaks. The fit for the highest temperature measured (1531 K) is only based on 9 peaks. At this point, most peaks have disappeared. For temperatures in the $I4/mcm$ and $Imma$ fields, it was necessary to use starting values for the fits that were very close to the final fitted values. A calibration of G as a function of (frequency)^2 for the third resonance peak from the $Pnma$ phase was created based on the fact that the elastic constants of a material are directly proportional to the squares of the frequencies of its normal modes (Migliori and Sarrao 1997), and that the lowest frequency peaks are usually determined by almost pure shear modes. This calibration was found to match closely with data for the shear modulus, G, of the $Pm\bar{3}m$ phase and was therefore considered to give a reliable determination of G for the $I4/mcm$ and $Imma$ phases when only a small number of peaks could be observed. These values for G were then used as the starting values of fits for the $I4/mcm$ and $Imma$ phases.

It is evident from figure 2(c) that the elastic constants, especially the shear modulus, are strongly affected by each of the three phase transitions in $SrZrO_3$. There is a large amount of elastic softening associated with each phase transition, with the $I4/mcm$ and $Imma$ phases being significantly softer (up to ∼50 GPa) than the $Pm\bar{3}m$ and $Pnma$ phases. From the perspective of elasticity alone, the properties of the $Pm\bar{3}m$ and $Pnma$ phases are rather similar.

3.3. Experimental uncertainties

For low temperature measurements, the temperature stability at each equilibration step is approximately ±0.1 K. Using the high temperature RUS system, the estimated precision is approximately ±0.3 K for temperatures below 1255 K and approximately ±1 K for temperatures above 1255 K. As the transition temperatures in this study are estimated from breaks in slope of frequencies of RUS spectra collected at 1 K intervals, there is also an error on each value of at least ±1 K.

As stated earlier, the parallelepiped used for all measurements was cut from a sintered pellet with ∼2.8% porosity. This porosity has some effect on the absolute values of elastic moduli. A correction can be applied to give a value for 0% porosity using the expressions given by Ledbetter *et al* (1994). Using this correction, room temperature values, measured from the raw data as $K = 147.5$ GPa and $G = 84.52$ GPa, become $K = 157.37$ GPa and $G = 89.26$ GPa for a 100% dense sample. A similar correction could be applied to all the data but has not been carried out in this analysis, as the

form of the relative effects of the phase transitions on elastic moduli can be seen clearly in the uncorrected data (figure 2(c)). No correction for thermal expansion has been applied, for the same reasons.

Absolute values for elastic moduli are also influenced by the number of measured resonance peaks used for the fitting process. The more peaks that can be fitted, the more robust the refinement. The quality of the fit between calculated and observed resonance frequencies is quoted in the output DRS fitting file as a RMS (root mean square) error percentage. The estimated errors in K and G associated with the fit are also given in the output file. Where ~20 peaks were used for fitting (up to 900 K and above 1365 K), RMS errors are between 0.25 and 0.5% and uncertainties in K and G are 0.5–1% and 0.1–0.2% respectively. These values imply a 'good fit', following Migliori and Sarrao (1997). Between 900 K and 1365 K, when only 5–10 peaks are used for the fit, RMS errors are between 0.5 and 1% with uncertainties in K and G being 1–5% and 0.2–0.3% respectively, with the largest uncertainties being at each of the phase transition temperatures. The important point to note here is that G is relatively well constrained across the whole temperature range, whereas K shows a much larger variation in uncertainties, especially in the $Imma$ and $I4/mcm$ stability fields. Such uncertainties are not shown in figure 2(c) as they are well within the bounds of the symbol size for values of G and only up to the size of the symbols for K.

4. Strain analysis

Variations of elastic constants associated with octahedral tilting transitions in perovskites arise largely as a consequence of strain/order parameter coupling. Formal relationships between spontaneous strains and individual order parameter components described by Landau theory provide a measure of the evolution of a structure across multi order parameter space. They can also be used to extract expressions for the evolution of individual elastic constants or of bulk elastic properties. In this context, combinations of M- and R-point tilts are expected to conform to relationships derived from a Landau expansion of the form (Carpenter *et al* 2001, Carpenter 2007):

$$\begin{aligned}
G = {} & \tfrac{1}{2}a_1\Theta_{s1}\left(\coth\left(\frac{\Theta_{s1}}{T}\right) - \coth\left(\frac{\Theta_{s1}}{T_{c1}}\right)\right)\left(q_1^2+q_2^2+q_3^2\right) \\
& + \tfrac{1}{2}a_2\Theta_{s2}\left(\coth\left(\frac{\Theta_{s2}}{T}\right) - \coth\left(\frac{\Theta_{s2}}{T_{c2}}\right)\right)\left(q_4^2+q_5^2+q_6^2\right) \\
& + \tfrac{1}{4}b_1\left(q_1^2+q_2^2+q_3^2\right)^2 + \tfrac{1}{4}b_1'\left(q_1^4+q_2^4+q_3^4\right) \\
& + \tfrac{1}{4}b_2\left(q_4^2+q_5^2+q_6^2\right)^2 + \tfrac{1}{4}b_2'\left(q_4^4+q_5^4+q_6^4\right) \\
& + \tfrac{1}{6}c_1\left(q_1^2+q_2^2+q_3^2\right)^3 + \tfrac{1}{6}c_1'\left(q_1q_2q_3\right)^2 \\
& + \tfrac{1}{6}c_1''\left(q_1^2+q_2^2+q_3^2\right)\left(q_1^4+q_2^4+q_3^4\right) \\
& + \tfrac{1}{6}c_2\left(q_4^2+q_5^2+q_6^2\right)^3 + \tfrac{1}{6}c_2'\left(q_4q_5q_6\right)^2 \\
& + \tfrac{1}{6}c_2''\left(q_4^2+q_5^2+q_6^2\right)\left(q_4^4+q_5^4+q_6^4\right) \\
& + \lambda_q\left(q_1^2+q_2^2+q_3^2\right)\left(q_4^2+q_5^2+q_6^2\right) \\
& + \lambda_q'\left(q_1^2q_4^2+q_2^2q_5^2+q_3^2q_6^2\right) \\
& + \lambda_1 e_a\left(q_1^2+q_2^2+q_3^2\right) + \lambda_2 e_a\left(q_4^2+q_5^2+q_6^2\right) \\
& + \lambda_3\left[\sqrt{3}e_{oz}\left(q_2^2-q_3^2\right) + e_{tz}\left(2q_1^2-q_2^2-q_3^2\right)\right] \\
& + \lambda_4\left[\sqrt{3}e_{oz}\left(q_5^2-q_6^2\right) + e_{tz}\left(2q_4^2-q_5^2-q_6^2\right)\right] \\
& + \lambda_5\left(e_4q_4q_6 + e_5q_4q_5 + e_6q_5q_6\right) \\
& + \lambda_6\left(q_1^2+q_2^2+q_3^2\right)\left(e_4^2+e_5^2+e_6^2\right) \\
& + \lambda_7\left(q_1^2e_6^2+q_2^2e_4^2+q_3^2e_5^2\right) \\
& + \tfrac{1}{4}\left(C_{11}^0-C_{12}^0\right)\left(e_{oz}^2+e_{tz}^2\right) + \tfrac{1}{6}\left(C_{11}^0+2C_{12}^0\right)e_a^2 \\
& + \tfrac{1}{2}C_{44}^0\left(e_4^2+e_5^2+e_6^2\right). \qquad (2)
\end{aligned}$$

$I4/mcm$, $Imma$ and $Pnma$ structures have $q_4 \neq 0$ ($q_1 = q_2 = q_3 = q_5 = q_6 = 0$), $q_4 = q_6 \neq 0$ ($q_1 = q_2 = q_3 = q_5 = 0$) and $q_4 = q_6 \neq 0$, $q_2 \neq 0$ ($q_1 = q_3 = q_5 = 0$), respectively, for the relationships between crystallographic axes and the orthogonal reference axes, X, Y, Z, specified in figure 1 of Carpenter (2007). a_1, a_2, b_1, etc, are normal Landau coefficients; Θ_{s1}, Θ_{s2} are saturation temperatures; T_{c1}, T_{c2} are critical temperatures; λ_1, λ_q, etc, are coupling coefficients; C_{11}^0, C_{12}^0, C_{44}^0 are bare elastic constants; and e_4, e_5, e_6 are shear strain components. The symmetry-adapted strains, e_a, e_{oz} and e_{tz} are combinations of the linear strain components e_1, e_2 and e_3 as

$$e_a = (e_1 + e_2 + e_3) \qquad (3)$$

$$e_{oz} = (e_1 - e_2) \qquad (4)$$

$$e_{tz} = \frac{1}{\sqrt{3}}(2e_3 - e_1 - e_2). \qquad (5)$$

A subscript z has been included to indicate that the tetragonal and orthorhombic shear strains, e_{tz} and e_{oz}, are specified for the unique direction being parallel to Z. For $Imma$ and $Pnma$ structures, it is convenient to specify the unique axis of the tetragonal strain as being parallel to X, in which case the symmetry breaking strains are defined as:

$$e_{ox} = (e_2 - e_3) \qquad (6)$$

$$e_{tx} = \frac{1}{\sqrt{3}}(2e_1 - e_2 - e_3). \qquad (7)$$

Setting equilibrium conditions of the form $\partial G/\partial e = 0$ then gives the strain/order parameter relationships listed in table 2.

Lattice parameter data for $SrZrO_3$ obtained by Howard *et al* (2000) using high resolution powder neutron diffraction are reproduced in figure 3(a), and have been used to determine the evolution of individual strains. Variations of spontaneous strains calculated from these for $I4/mcm$, $Imma$ and $Pnma$ structures, using the expressions given in table 2, are shown in figure 3(b). The reference parameter a_0 represents the lattice parameter of the cubic phase extrapolated from high temperatures, as specified by (after Salje *et al* 1991, Meyer *et al* 2000, 2001, Sondergeld *et al* 2000, Carpenter *et al* 2003):

$$a_0 = a_1 + a_2\Theta_{os}\coth\left(\frac{\Theta_{os}}{T}\right). \qquad (8)$$

The saturation temperature, Θ_{os}, was set arbitrarily to 150 K in order to introduce some more or less realistic curvature as $T \to 0$ K. A fit to the lattice parameters for the cubic phase then gave $a_1 = 4.0869$ Å, $a_2 = 4.8848 \times 10^{-5}$ Å K^{-1}.

Table 2. Relationships between spontaneous strains and order parameter components of $I4/mcm$, $Imma$ and $Pnma$ structures, as derived by applying the equilibration condition $\partial G/\partial e = 0$ to equation (2). Definitions of the strain components, e_1–e_4, in terms of the lattice parameters, a, b, and c, are reproduced from Carpenter *et al* (2001); a_0 is the reference lattice parameter of the parent cubic phase.

$I4/mcm$	$Imma$	$Pnma$
$e_a = -\dfrac{\lambda_2 q_4^2}{\frac{1}{3}(C_{11}^0 + 2C_{12}^0)}$	$e_a = -\dfrac{2\lambda_2 q_4^2}{\frac{1}{3}(C_{11}^0 + 2C_{12}^0)}$	$e_a = -\dfrac{(\lambda_1 q_2^2 + 2\lambda_2 q_4^2)}{\frac{1}{3}(C_{11}^0 + 2C_{12}^0)}$
$e_{oz} = 0$	$e_{ox} = 0$	$e_{ox} = 0$
$e_{tz} = -\dfrac{2\lambda_4 q_4^2}{\frac{1}{2}(C_{11}^0 - C_{12}^0)}$	$e_{tx} = \dfrac{2\lambda_4 q_4^2}{\frac{1}{2}(C_{11}^0 - C_{12}^0)}$	$e_{tx} = -\dfrac{2(\lambda_3 q_2^2 - \lambda_4 q_4^2)}{\frac{1}{2}(C_{11}^0 - C_{12}^0)}$
$e_4 = e_5 = e_6 = 0$	$e_4 = -\dfrac{\lambda_5 q_4^2}{C_{44}^0}$	$e_4 = -\dfrac{\lambda_5 q_4^2}{2q_2^2(\lambda_6 + \lambda_7) + C_{44}^0}$
	$e_5 = e_6 = 0$	$e_5 = e_6 = 0$
$e_1 = e_2 = \dfrac{\frac{a}{\sqrt{2}} - a_0}{a_0}$	$e_1 = \dfrac{\frac{b}{2} - a_0}{a_0}$	$e_1 = \dfrac{\frac{b}{2} - a_0}{a_0}$
$e_3 = \dfrac{\frac{c}{2} - a_0}{a_0}$	$e_2 + e_3 = \dfrac{\frac{a}{\sqrt{2}} - a_0}{a_0} + \dfrac{\frac{c}{\sqrt{2}} - a_0}{a_0}$	$e_2 + e_3 = \dfrac{\frac{a}{\sqrt{2}} - a_0}{a_0} + \dfrac{\frac{c}{\sqrt{2}} - a_0}{a_0}$
	$e_4 = \dfrac{\frac{a}{\sqrt{2}} - a_0}{a_0} - \dfrac{\frac{c}{\sqrt{2}} - a_0}{a_0}$	$e_4 = \dfrac{\frac{a}{\sqrt{2}} - a_0}{a_0} - \dfrac{\frac{c}{\sqrt{2}} - a_0}{a_0}$

Variations of the volume strain e_a are sensitive to the choice of a_0, but values of shear strains are relatively independent of this fitting process.

The square of the tetragonal strain, e_{tz}, varies linearly with temperature in the stability field of the $I4/mcm$ structure (figure 3(c)), implying that the $Pm\bar{3}m \leftrightarrow I4/mcm$ transition is close to being tricritical in character, with $T_{c2} = 1342$ K ($e_{tz}^2 \propto q_4^4 \propto (T_c - T)$). The $Imma$ structure develops by a first order transition from the $I4/mcm$ structure, but is related to the $Pm\bar{3}m$ structure by the same instability and tricritical evolution, as shown by the linear temperature dependence of e_{tx}^2 (figure 3(c)). The $Pnma$ structure develops from the $Imma$ structure by a continuous change in lattice parameters at 1018 K, and the deviation of e_{tx} from the trend established in the $Imma$ stability field provides a measure of q_2^2 (see table 2). If it is assumed that q_4 and q_2 are only weakly coupled, such that q_4 has the same temperature dependence in the $Pnma$ structure as it does in the $Imma$ structure, the change in e_{tx} ('e_{tx}, excess' in figure 3(b)) provides a measure of q_2^2. Figure 3(d) shows that (e_{tx}, excess)^2 varies linearly with temperature over a significant temperature interval below 1018 K, consistent with $q_2^4 \propto T$ and close to tricritical character for the $Imma \leftrightarrow Pnma$ transition. The $Imma$ structure has e_4 close to zero, implying that the coupling coefficient λ_5 is small. This shear strain would be expected to show the same dependence on q_4 in the $Pnma$ stability field since, to a good approximation, C_{44}^0 is expected to be substantially greater than $2q_2^2(\lambda_6 + \lambda_7)$. However, e_4 increases markedly (figure 3(b)) with decreasing temperature, as if λ_5 is itself temperature dependent. The variation of $e_4^{0.5}$ with temperature is not far from being linear (figure 3(e)) and one possible explanation of this behaviour is that λ_5 is sensitive to the degree of M-point tilting, say as $\lambda_5 \propto q_2^2$ or $\lambda_5 \propto q_2^4$. The physical origin of such an effect could lie in the fact that the octahedra are not rigid units and deform as they tilt; deformation of the octahedra associated with M-point tilting would change the amount of geometrical strain associated with R-point tilting. Distortions of the octahedra are presumably responsible also for the unusual evolution of the volume strain, e_a, which changes sign from negative to positive with falling temperature and is close to zero in the $Imma$ stability field (figure 3(b)).

Tilt angles extracted from the original neutron powder diffraction data of Howard *et al* (2000) confirm these strain/order parameter relationships. Figure 3(f) contains e_t^2 (left axis) and ϕ^4 (right axis), where ϕ is the R-point tilt angle, scaled so that the data points overlap. The tilt angles scale as $\phi^2 \propto e_t$, with a constant ratio for the $Imma$ and $I4/mcm$ structures. The M-point tilt angle, φ, varies approximately as $\varphi^4 \propto (T_c - T)$, within reasonable experimental uncertainty (figure 3(g)), consistent with the view that the $Imma \leftrightarrow Pnma$ transition is also close to being tricritical in character. ϕ^4 varies continuously through this transition without an obvious break in slope (figure 3(g)), implying that coupling between the M-point and R-point tilts in the $Pnma$ structure is indeed weak.

5. Predicted form of the elastic anomalies

The underlying mechanism of elastic softening due to octahedral tilting transitions in perovskites is well understood. An externally applied stress causes a lattice distortion according to Hooke's law. There is then an additional relaxation as the tilt angles respond to the change in strain through the strain/order parameter coupling coefficients. This relaxation is described formally by the widely used expression for individual elastic constants, C_{ik}, given by Slonczewski and Thomas (1970):

$$C_{ik} = C_{ik}^0 - \sum_{l,m} \frac{\partial^2 G}{\partial e_i \partial q_l} R_{lm} \frac{\partial^2 G}{\partial e_k \partial q_m}, \qquad (9)$$

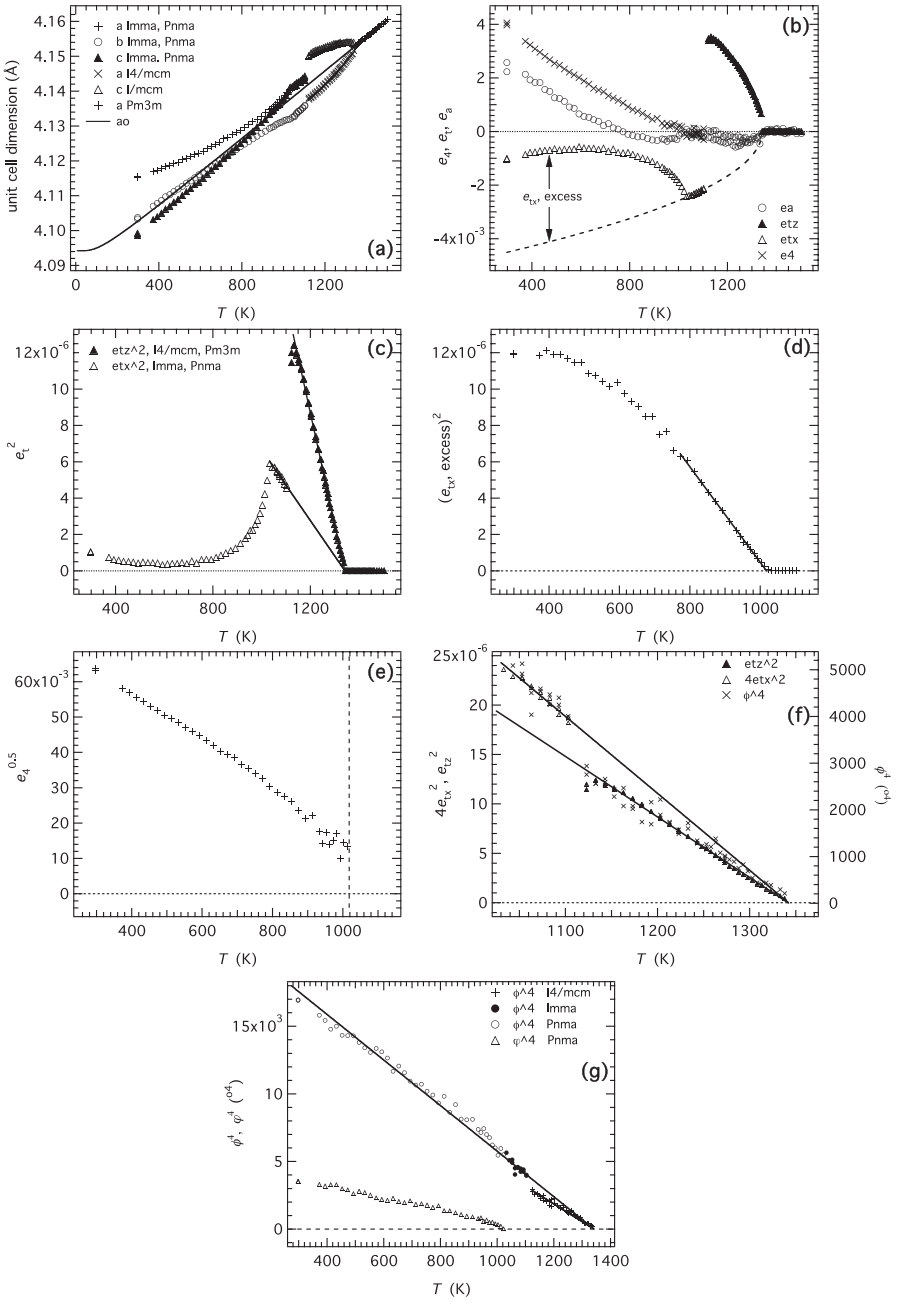

Figure 3. Strain analysis of lattice parameter data from Howard *et al* (2000). (a) Lattice parameters of the reduced unit cell. The solid line is a fit of equation (8) to data for the cubic phase, with $\Theta_{os} = 150$ K. (b) Spontaneous strains calculated using the expressions listed in table 2. The broken line is a fit to e_{tx} for the *Imma* structure as $e_{tx}^2 \propto T$. (c) The square of the tetragonal strains varies linearly with temperature across the stability fields of the $I4/mcm$ and *Imma* structures and extrapolates to zero at the same instability temperature. This is consistent with tricritical character for $Pm\bar{3}m \leftrightarrow I4/mcm$ and $Pm\bar{3}m \leftrightarrow Imma$ transitions with $T_{c2} = 1342$ K. (d) The excess tetragonal strain from (b) varies as $e_{tx}^2 \propto T$ for a wide temperature interval below the $Imma \leftrightarrow Pnma$ transition point, consistent with tricritical character for this transition. (e) The strain e_4 has an unusual temperature dependence in (b) which corresponds approximately to $e_4^{0.5} \propto T$ in the *Pnma* stability field. (f) e_t^2 (left axis) and ϕ^4 (right axis) show the same linear temperature dependence in the $I4/mcm$ and *Imma* structures, consistent with $e_t \propto \phi^2 (\propto q_4^2)$ in both. (g) ϕ^4 and φ^4 scale approximately linearly with temperature, consistent with an approximately tricritical evolution of both. There is no obvious break in slope or discontinuity in the temperature dependence of ϕ at the $Imma \leftrightarrow Pnma$ transition, consistent with there being only weak coupling between the M-point and R-point order parameters in the *Pnma* structure.

where C_{ik}^0 are the bare elastic constants. The matrix, R_{lm}, is the inverse of the matrix, $\frac{\partial^2 G}{\partial q_l \partial q_m}$, i.e.

$$\sum_m R_{lm} \frac{\partial^2 G}{\partial q_m \partial q_n} = \delta_{ln}. \tag{10}$$

For almost all cases examined in the literature, the matrix $\frac{\partial^2 G}{\partial q_l \partial q_m}$ and hence R_{lm} contain only diagonal terms. Equation (9) is often given in a simplified form, therefore, such as

$$C_{ik} = C_{ik}^0 - \sum_m \frac{\partial^2 G}{\partial e_i \partial q_m} \left(\frac{\partial^2 G}{\partial q_m^2} \right)^{-1} \frac{\partial^2 G}{\partial e_k \partial q_m}. \tag{11}$$

Table 3. Elastic constant variations expected in the stability field of a structure with $I4/mcm$ symmetry ($q_4 \neq 0, q_5 = q_6 = 0$), due to a transition from a parent cubic structure with $Pm\bar{3}m$ symmetry.

$C_{11} = C_{22} = C_{11}^0 - M^2 R_{44} q_4^2$	$C_{13} = C_{23} = C_{12}^0 - MNR_{44} q_4^2$
$C_{33} = C_{11}^0 - N^2 R_{44} q_4^2$	$C_{44} = C_{55} = C_{44}^0 - \lambda_5^2 R_{66} q_4^2$
$C_{12} = C_{12}^0 - M^2 R_{44} q_4^2$	$C_{66} = C_{44}^0$
[a] $K_V = \frac{1}{3}(C_{11}^0 + 2C_{12}^0) - 4\lambda_2^2 R_{44} q_4^2$	
[a] $G_V = \frac{1}{5}(C_{11}^0 - C_{12}^0 + 3C_{44}^0) - \frac{2}{5}(8\lambda_4^2 R_{44} + \lambda_5^2 R_{66}) q_4^2$	
$R_{44} = \frac{1}{G_{44}}$	$R_{66} = \frac{1}{G_{66}}$
$G_{44} = \partial^2 G/\partial q_4^2 = 2(b_2 + b_2')q_4^2 + 4(c_2 + c_2'')q_4^4$	
$G_{66} = \partial^2 G/\partial q_6^2 = \left[\frac{12\lambda_4^2}{\frac{1}{2}(C_{11}^0 - C_{12}^0)} - b_2'\right] q_4^2 - \frac{2}{3} c_2'' q_4^4$	
$M = (2\lambda_2 - \frac{4}{\sqrt{3}}\lambda_4)$	$N = (2\lambda_2 + \frac{8}{\sqrt{3}}\lambda_4)$
Elastic constants, $C_{ik,c}$, for a unit cell with conventional orientation ($\mathbf{a} \parallel X, \mathbf{b} \parallel Y, \mathbf{c} \parallel Z$):	
$C_{11,c} = C_{22,c} = \frac{1}{2}(C_{11} + C_{12}) + C_{66}$	$C_{13,c} = C_{23,c} = C_{13}$
$C_{33,c} = C_{33}$	$C_{44,c} = C_{55,c} = C_{44}$
$C_{12,c} = \frac{1}{2}(C_{11} + C_{12}) - C_{66}$	$C_{66,c} = \frac{1}{2}(C_{11} - C_{12})$

[a] Expressions for the Voigt limits of bulk and shear modulus in terms of single crystal elastic constants for a crystal with $4/mmm$ symmetry were taken from Watt and Peselnik (1980).

The relaxation of individual elastic constants can have a variety of forms, depending on the nature of the relevant strain/order parameter coupling term and the thermodynamic character of the phase transition. For the simplest case of an improper ferroelastic transition a typical solution is $C = C^0 - \lambda^2 R q^2$. Whether the strain/order parameter coupling coefficient, λ, is positive or negative, lowering of the symmetry causes softening. R usually has the form $(Aq^2 + Bq^4)^{-1}$ so that the transition point is marked by a discontinuity in some of the elastic constants.

The reference system underlying equation (2) is that of the group theory program, ISOTROPY (Stokes and Hatch, Brigham Young University). Crystallographic orientations for $I4/mcm$, $Imma$ and $Pnma$ structures with respect to this reference system are shown in Carpenter (2007). Expressions for changes in elastic properties for each of these structures with respect to the parent $Pm\bar{3}m$ structure are listed in tables 3–6. Of principal interest in the present context are the bulk modulus, K, and shear modulus, G. The simplest form of these is given by the Voigt limits, K_V and G_V, which are included to show the role of specific strain/order parameter coupling terms. K_V is not likely to differ greatly from the Reuss limit of the bulk modulus, K_R, so the expressions provided are probably good representations of the expected elastic anomalies in K. The Reuss limit of the shear modulus, G_R, will be significantly different from the Voigt limit, however, so that the expressions for G_V provide only qualitative representations of the evolution of G. These expressions confirm that both K and G are expected to soften as a consequence of $Pm\bar{3}m \leftrightarrow I4/mcm$ and $Pm\bar{3}m \leftrightarrow Imma$ transitions. From the analysis above, it is apparent that λ_5 is small in $SrZrO_3$, so any observed softening of the shear modulus can be attributed mainly to coupling of order parameter components with the tetragonal strain.

The $I4/mcm$ and $Imma$ structures of $SrZrO_3$ are related to the cubic parent structure via the same instability and have an order parameter evolution characteristic of near tricritical behaviour. Their evolution is expected to follow solutions to

Table 4. Elastic constant variations expected in the stability field of a structure with $Imma$ symmetry ($q_4 = q_6 \neq 0, q_5 = 0$), due to a transition from a parent cubic structure with $Pm\bar{3}m$ symmetry.

$C_{11} = C_{11}^0 - 2M^2(R_{44} + R_{46})q_4^2$	$C_{55} = C_{66} = C_{44}^0 - \lambda_5^2 R_{55} q_4^2$
$C_{22} = C_{33} = C_{11}^0 - [(M^2 + N^2)R_{44} + 2MNR_{46}]q_4^2$	$C_{14} = -2M\lambda_5(R_{44} + R_{46})q_4^2$
$C_{12} = C_{13} = C_{12}^0 - (M^2 + MN)(R_{44} + R_{46})q_4^2$	$C_{24} = C_{34} = -(M + N)\lambda_5(R_{44} + R_{46})q_4^2$
$C_{23} = C_{12}^0 - [2MNR_{44} + (M^2 + N^2)R_{46}]q_4^2$	$C_{56} = -\lambda_5^2 R_{55} q_4^2$
$C_{44} = C_{44}^0 - 2\lambda_5^2(R_{44} + R_{46})q_4^2$	
[a] $K_V = \frac{1}{3}(C_{11}^0 + 2C_{12}^0) - 8\lambda_2^2(R_{44} + R_{46})q_4^2$	
[a] $G_V = \frac{1}{5}(C_{11}^0 - C_{12}^0 + 3C_{44}^0) - \frac{2}{5}(8\lambda_4^2(2R_{44} - R_{46}) + \lambda_5^2(R_{44} + R_{46} + R_{55}))q_4^2$	
$R_{44} = R_{66} = \frac{G_{44}}{G_{44}^2 - G_{46}^2}$,	$R_{46} = \frac{-G_{46}}{G_{44}^2 - G_{46}^2}$, $R_{55} = \frac{1}{G_{55}}$
$G_{44}(= G_{66}) = \partial^2 G/\partial q_4^2 = \left(2b_2 + 2b_2' + \frac{\lambda_5^2}{C_{44}^0}\right)q_4^2 + 8(c_2 + \frac{2}{3}c_2'')q_4^4$	
$G_{55} = \partial^2 G/\partial q_5^2 = \left[\frac{\lambda_5^2}{C_{44}^0} + \frac{12\lambda_4^2}{\frac{1}{2}(C_{11}^0 - C_{12}^0)} - b_2'\right]q_4^2 + \frac{1}{3}(c_2' - 4c_2'')q_4^4$	
$G_{46} = \partial^2 G/\partial q_4 \partial q_6 = \left(2b_2 - \frac{\lambda_5^2}{C_{44}^0}\right)q_4^2 + 8(c_2 + \frac{1}{3}c_2'')q_4^4$	
Elastic constants, $C_{ik,c}$, for a unit cell with conventional orientation ($\mathbf{a} \parallel X, \mathbf{b} \parallel Y, \mathbf{c} \parallel Z$):	
$C_{11,c} = \frac{1}{2}(C_{22} + C_{23}) + 2C_{24} + C_{44}$	$C_{23,c} = C_{12} - C_{14}$
$C_{22,c} = C_{11}$	$C_{44,c} = \frac{1}{2}(C_{55} + C_{66}) - C_{56}$
$C_{33,c} = \frac{1}{2}(C_{22} + C_{23}) - 2C_{24} + C_{44}$	$C_{55,c} = \frac{1}{2}(C_{22} - C_{23})$
$C_{12,c} = C_{12} + C_{14}$	$C_{66,c} = \frac{1}{2}(C_{55} + C_{66}) + C_{56}$
$C_{13,c} = \frac{1}{2}(C_{22} + C_{23}) - C_{44}$	

[a] Expressions for the Voigt limits of bulk and shear modulus in terms of single crystal constants for an orthorhombic crystal were taken from Watt (1979).

Table 5. Elastic constant variations expected in the stability field of a structure with $P4/mbm$ symmetry ($q_2 \neq 0, q_1 = q_3 = 0$), due to a transition from a parent cubic structure with $Pm\bar{3}m$ symmetry.

$C_{11} = C^0_{11} - P^2 R_{22} q_2^2$	$C_{23} = C^0_{12} - O^2 R_{22} q_2^2$
$C_{22} = C_{33} = C^0_{11} - O^2 R_{22} q_2^2$	$C_{44} = C^0_{44} + 2(\lambda_6 + \lambda_7) q_2^2$
$C_{12} = C_{13} = C^0_{12} - O P R_{22} q_2^2$	$C_{55} = C_{66} = C^0_{44} + 2\lambda_6 q_2^2$
[a] $K_V = \frac{1}{3}(C^0_{11} + 2C^0_{12}) - 4\lambda_1^2 R_{22} q_2^2$	
[a] $G_V = \frac{1}{5}(C^0_{11} - C^0_{12} + 3C^0_{44}) - \frac{2}{5}(8\lambda_3^2 R_{22} - 3\lambda_6 - 2\lambda_7) q_2^2$	
$R_{22} = \frac{1}{G_{22}}$	
$G_{22} = \partial^2 G / \partial q_2^2 = 2(b_1 + b_1') q_2^2 + 4(c_1 + c_1'') q_2^4$	
$O = (2\lambda_1 - \frac{4}{\sqrt{3}}\lambda_3)$	$P = (2\lambda_1 + \frac{8}{\sqrt{3}}\lambda_3)$
Elastic constants, $C_{ik,c}$, for a unit cell with conventional orientation ($\mathbf{a} \parallel X, \mathbf{b} \parallel Y, \mathbf{c} \parallel Z$):	
$C_{11,c} = C_{22,c} = \frac{1}{2}(C_{22} + C_{23}) + C_{44}$	$C_{13,c} = C_{23,c} = C_{12}$
$C_{33,c} = C_{11}$	$C_{44,c} = C_{55,c} = C_{55}$
$C_{12,c} = \frac{1}{2}(C_{22} + C_{23}) - C_{44}$	$C_{66,c} = \frac{1}{2}(C_{22} - C_{23})$

[a] Expressions for the Voigt limits of bulk and shear modulus in terms of single crystal elastic constants for a crystal with $4/mmm$ symmetry were taken from Watt and Peselnik (1980).

the renormalized form of equation (2):

$$G = \frac{1}{2} a_2 \Theta_{s2} \left(\coth\left(\frac{\Theta_{s2}}{T}\right) - \coth\left(\frac{\Theta_{s2}}{T_{c2}}\right) \right) \left(q_4^2 + q_5^2 + q_6^2\right) + \tfrac{1}{4} b_2^* \left(q_4^2 + q_5^2 + q_6^2\right)^2 + \tfrac{1}{4} b_2'^* \left(q_4^4 + q_5^4 + q_6^4\right) + \tfrac{1}{6} c_2 \left(q_4^2 + q_5^2 + q_6^2\right)^3 + \tfrac{1}{6} c_2' (q_4 q_5 q_6)^2 + \tfrac{1}{6} c_2'' \left(q_4^2 + q_5^2 + q_6^2\right)\left(q_4^4 + q_5^4 + q_6^4\right) \quad (12)$$

where

$$b_2^* = b_2 - \frac{\lambda_5^2}{C^0_{44}} - \frac{2\lambda_2^2}{\frac{1}{3}\left(C^0_{11} + 2C^0_{12}\right)} + \frac{4\lambda_4^2}{\frac{1}{2}\left(C^0_{11} - C^0_{12}\right)} \approx 0 \quad (13)$$

$$b_2'^* = b_2' + \frac{\lambda_5^2}{C^0_{44}} - \frac{12\lambda_4^2}{\frac{1}{2}\left(C^0_{11} - C^0_{12}\right)} \approx 0. \quad (14)$$

Solutions for the temperature dependence of q_4 in the $I4/mcm$ and $Imma$ stability fields are then, respectively,

$$q_4^4 = \frac{a_2 \Theta_{s2} \left(\coth\left(\frac{\Theta_{s2}}{T_{c2}}\right) - \coth\left(\frac{\Theta_{s2}}{T}\right) \right)}{\left(c_2 + c_2''\right)} \quad (15)$$

$$4q_4^4 = \frac{a_2 \Theta_{s2} \left(\coth\left(\frac{\Theta_{s2}}{T_{c2}}\right) - \coth\left(\frac{\Theta_{s2}}{T}\right) \right)}{\left(c_2 + \frac{1}{2}c_2''\right)}. \quad (16)$$

Note that, because of the difference between one dimensional and two dimensional order parameters in the $I4/mcm$ and $Imma$ structures, the absolute value of q_4^2 in the $Imma$ structure is half the value of q_4^2 in the $I4/mcm$ structure. The actual evolution of the two structures is therefore almost identical apart from the small difference introduced in the denominator. This is consistent with the observed behaviour of $SrZrO_3$, as shown by replotting of the tetragonal strains and tilt angles in figure 3(f). When a tricritical solution for q_4 is substituted into the expressions for G_V, K_V, R_{44}, R_{55}, and R_{46}, the well known form of softening illustrated in figure 4 is predicted. The $I4/mcm \leftrightarrow Imma$ transition is expected to be marked only by a small discontinuity in K and G, without any premonitory softening as the transition point is approached from either side.

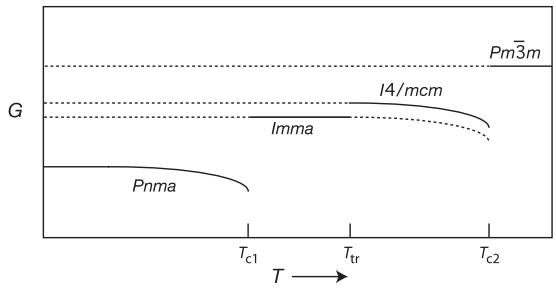

Figure 4. Schematic variation of shear modulus, G, expected on the basis of Landau theory for tricritical $Pm\bar{3}m \leftrightarrow I4/mcm$, $Pm\bar{3}m \leftrightarrow Imma$ and $Imma \leftrightarrow Pnma$ transitions (tables 3–6) with critical temperatures of T_{c2} and T_{c1}. The first order transition between $I4/mcm$ and $Imma$ structures at T_{tr} is expected to show only a small discontinuity.

The $Imma \leftrightarrow Pnma$ transition can be understood in terms of the evolution of q_2 below an M-point instability. In one limiting case, this would simply produce a second softening event described by the elastic constants listed in table 5. If q_2 follows a tricritical temperature dependence, the form should be similar to softening at the R-point instability, giving the sequence of elastic anomalies illustrated in figure 4. However, q_2 and q_4 are coupled, either directly through the coupling terms $\lambda_q(q_1^2 + q_2^2 + q_3^2)(q_4^2 + q_5^2 + q_6^2) + \lambda_q'(q_1^2 q_4^2 + q_2^2 q_5^2 + q_3^2 q_6^2)$ in equation (2) or indirectly via common strains. Applying an external stress to the $Pnma$ structure should therefore produce relaxations in both q_2 and q_4, though with potentially different consequences for the elastic constants from the single instabilities considered previously in the literature. In order to examine this behaviour in more detail, it is necessary to apply the Slonczewski and Thomas (1970) equation to 6 × 6 matrices and to consider all possible cross terms. Formal analysis of equation (2) on this basis gives the expressions listed in table 6. Whereas the pure M-point ($P4/mbm$) and R-point ($I4/mcm$, $Imma$) instabilities should give changes in elastic constants which depend predominantly on $-\lambda_1^2$, $-\lambda_2^2$, $-\lambda_3^2$ or $-\lambda_4^2$, expressions for the $Pnma$ structures can contain terms in $-\lambda_1\lambda_2$ and $-\lambda_3\lambda_4$ which might be positive or negative. This means that the $Imma \rightarrow Pnma$ transition could be accompanied by a degree of elastic stiffening. However, λ_1 and λ_2 are evidently small and, from the variation of e_{tx} with temperature, λ_3 and λ_4 both have the same sign. Furthermore, with the exception of $\frac{\partial^2 G}{\partial q_2 \partial q_4}$, which equals $4\lambda_q q_2 q_4$, the individual second derivatives of G have the form $Aq^2 + Bq^4$. A numerical analysis would be needed to show for certain that the overall influence on K_V and G_V would be softening, but the form of all the expressions in table 6 leads to the expectation of a discontinuous softening sequence with the general form shown in figure 4. Terms in λ_6 and λ_7 could influence the curvature below T_{c2} but would not eliminate the discontinuity.

Table 6. Elastic constant variations expected in the stability field of a structure with $Pnma$ symmetry ($q_2 \neq q_4 = q_6 \neq 0$, $q_1 = q_3 = q_5 = 0$), due to a transition from a parent cubic structure with $Pm\bar{3}m$ symmetry.

$C_{11} = C^0_{11} - P^2R_{22}q_2^2 - 2M^2(R_{44} + R_{46})q_4^2 - 4PMq_2q_4R_{24}$

$C_{22} = C_{33} = C^0_{11} - O^2R_{22}q_2^2 - [(M^2 + N^2)R_{44} + 2MNR_{46}]q_4^2 - 2(OM + ON)q_2q_4R_{24}$

$C_{12} = C_{13} = C^0_{12} - OPR_{22}q_2^2 - (M^2 + MN)(R_{44} + R_{46})q_4^2 - (2OM + PN + PM)q_2q_4R_{24}$

$C_{23} = C^0_{12} - O^2R_{22}q_2^2 - [2MNR_{44} + (M^2 + N^2)R_{46}]q_4^2 - 2(OM + ON)q_2q_4R_{24}$

$C_{14} = -2M\lambda_5(R_{44} + R_{46})q_4^2 - 2P\lambda_5q_2q_4R_{24}$

$C_{24} = C_{34} = -(M + N)\lambda_5(R_{44} + R_{46})q_4^2 - 2O\lambda_5q_2q_4R_{24}$

$C_{44} = C^0_{44} + 2(\lambda_6 + \lambda_7)q_2^2 - 2\lambda_5^2(R_{44} + R_{46})q_4^2$

$C_{55} = C_{66} = C^0_{44} + 2\lambda_6q_2^2 - \lambda_5^2R_{55}q_4^2$

$C_{56} = -\lambda_5^2R_{55}q_4^2$

[a] $K_V = \frac{1}{3}(C^0_{11} + 2C^0_{12}) - 4\lambda_1^2R_{22}q_2^2 - 8\lambda_2^2(R_{44} + R_{46})q_4^2 - \lambda_1\lambda_2q_2q_4R_{24}$

[a] $G_V = \frac{1}{5}(C^0_{11} - C^0_{12} + 3C^0_{44}) - \frac{2}{5}(8\lambda_3^2R_{22} - 3\lambda_6 - 2\lambda_7)q_2^2$
$-\frac{2}{5}(8\lambda_4^2(2R_{44} - R_{46}) + \lambda_5^2(R_{44} + R_{46} + R_{55}))q_4^2 + \frac{32}{5}\lambda_3\lambda_4q_2q_4R_{24}$

Elastic constants, $C_{ik,c}$, for a unit cell with conventional orientation ($\mathbf{a} \parallel X$, $\mathbf{b} \parallel Y$, $\mathbf{c} \parallel Z$):

$C_{11,c} = \frac{1}{2}(C_{22} + C_{23}) + 2C_{24} + C_{44}$ $\quad C_{23,c} = C_{12} - C_{14}$

$C_{22,c} = C_{11}$ $\quad C_{44,c} = \frac{1}{2}(C_{55} + C_{66}) - C_{56}$

$C_{33,c} = \frac{1}{2}(C_{22} + C_{23}) - 2C_{24} + C_{44}$ $\quad C_{55,c} = \frac{1}{2}(C_{22} - C_{23})$

$C_{12,c} = C_{12} + C_{14}$ $\quad C_{66,c} = \frac{1}{2}(C_{55} + C_{66}) + C_{56}$

$C_{13,c} = \frac{1}{2}(C_{22} + C_{23}) - C_{44}$

R_{22}, R_{44}, R_{55}, R_{46}, R_{24} are components of the inverse of the matrix
$\{(G_{11}, 0, 0, 0, 0, 0), (0, G_{22}, 0, G_{24}, 0, G_{24}), (0, 0, G_{11}, 0, 0, 0),$
$(0, G_{24}, 0, G_{44}, 0, G_{46}), (0, 0, 0, 0, G_{55}, 0), (0, G_{24}, 0, G_{46}, 0, G_{44})\}$ where
$G_{ij} = \frac{\partial^2 G}{\partial q_i \partial q_j}$

[a] Expressions for the Voigt limits of bulk and shear modulus in terms of single crystal elastic constants for an orthorhombic crystal were taken from Watt (1979).

6. Discussion

6.1. Elastic behaviour

McKnight *et al* (2008) have recently shown that polycrystalline samples can remain coherent, without cracking, through phase transitions involving the development of significant spontaneous strains when the grain size is ~5 μm or less. The variations in elastic properties described here for $SrZrO_3$ can, therefore, be expected to be intrinsic to the grains themselves, rather than to the development of any microcracking or pull-apart along grain boundaries at the three phase transitions. A possible exception to this is the change in Q^{-1} observed at the highest temperatures in the stability field of the cubic phase. If this is due to sample degradation of some sort, it does not appear to have changed the rest of the elastic behaviour which was more or less reproducible in heating and cooling cycles, i.e. before and after heating to the highest temperatures.

Across the $Pm\bar{3}m \leftrightarrow I4/mcm$ transition, the evolution of elastic constants is as predicted for a tricritical phase transition. There is some softening ahead of the transition over a very narrow temperature region (~10 K) which is not included in the Landau model but this is a characteristic feature of phase transitions which can generally be understood in terms of fluctuations, as reviewed by Carpenter and Salje (1998), for example. The transition itself is marked by a discontinuity in both K and G, with softening of the $I4/mcm$ phase (figure 2(c)) having the same form as is shown schematically in figure 4. Similar large degrees of softening have also been observed at the $Pm\bar{3}m \leftrightarrow I4/mcm$ transition in the $(Ca,Sr)TiO_3$ perovskite system (Carpenter *et al* 2006, 2007, Walsh *et al* 2008). A more quantitative analysis will require full calibration of the Landau coefficients, as has been achieved for $SrTiO_3$ (Carpenter 2007).

The $I4/mcm \leftrightarrow Imma$ transition must necessarily be first order in character (Devonshire 1949,1951, Howard *et al* 2000). It marks a change from a one-component order parameter system to a two-component system and, from the strain analysis, $Imma$ is related to the cubic structure by the same instability as $I4/mcm$. Therefore, it is expected that there will simply be a small discontinuity in elastic properties at the transition point. This is not the case, however, as distinct softening is observed in both phases over a temperature interval of up to 100 K on either side of the transition. The clear implication of this is that there are premonitory effects in both the $Imma$ and $I4/mcm$ structures and that the transition does not simply involve a discontinuous switch from one phase to the other. The detailed mechanism of this transition is as yet unknown, but one possibility is that clustering of local regions of one tilt system occurs within the other on a dynamical basis. This pattern of softening is identical to that observed in $BaTiO_3$ (Cheng *et al* 1994, Zhang *et al* 1994) and may therefore be a universal feature of hierarchical sequences of phase transitions. In the case of $BaTiO_3$, Cheng *et al* (1994) observed 'anomaly-peak pairs' at each phase transition and attributed the sharper one to the transition, with the broader peak accompanying it suggested to be associated with twin-boundary or domain wall relaxation before the transition point.

What is most contrary to expectation in relation to the elastic behaviour of $SrZrO_3$ is the behaviour of K and G across the $Imma \leftrightarrow Pnma$ phase transition. Changes in both bulk and shear moduli are continuous and there is substantial stiffening in the $Pnma$ phase on cooling from the transition temperature, to the extent that the elastic constants return to the trend established for the cubic phase as if there had been no influence from any of the intermediate transitions. Strain analysis shows that the $Imma \leftrightarrow Pnma$ phase transition occurs by approximately tricritical development of M-point tilts and that coupling between M- and R-point tilts is weak. Therefore, the expectation is that the transition should be marked by a discontinuous drop in K and G as presented in figure 4. The experimentally observed stiffening implies that the strain/order parameter relaxation predicted by Landau theory is not operating in the $Pnma$ structure. In other words, application of a stress in the RUS frequency range (1 MHz) does not induce a relaxation of the tilts. Similar data were obtained for (Ca,Sr)TiO_3 (Carpenter *et al* 2006, 2007, Walsh *et al* 2008) where the orthorhombic phase is also unexpectedly stiffer than the tetragonal phase. The implication is that tilt responses to stress become impeded once two tilt systems operate together. It is not yet clear whether the same result would be obtained at zero frequency, i.e. it could be purely an effect of dispersion with respect to frequency; however, data of Harrison *et al* (2003) for (Ca,Sr)TiO_3 collected by dynamical mechanical analysis at 0.01–50 Hz show that Young's modulus of the $Pnma$ phase is only slightly smaller than for the cubic phase extrapolated to the same temperature.

The origin of this unexpected aspect of the elastic behaviour of $SrZrO_3$ is perhaps related to the unusual variation of the strain component, e_4, observed in the $Pnma$ stability field. The coupling coefficient, λ_5, appears to be a function of the magnitude of the M-point tilt. If this is due to distortion of the ZrO_6 units, the freedom of the octahedra to rotate in response to an applied stress might become impeded. Combined R-point plus M-point tilts would thus become constrained such that the elastic behaviour of the $Pnma$ structure is determined simply by bond compression, much as it is in the cubic phase. This would have important implications for silicate perovskites in the lower mantle which should behave as classically stiff materials independent of phase transitions at higher temperatures.

6.2. Dissipation behaviour

A peak in dissipation, Q^{-1} (shown in figure 2(b)), at the cubic $\leftrightarrow$ tetragonal transition is a common feature of displacive phase transitions and relates to the variation of susceptibility close the transition point (Rehwald 1973, Fossheim *et al* 1974, Lüthi and Rehwald 1981, Fossheim and Fossum 1984, Carpenter and Salje 1998, Schranz *et al* 1999, Kityk *et al* 2000). Within the tetragonal $I4/mcm$ stability field, Q^{-1} remains relatively high. This could be an intrinsic effect of coupling between octahedral tilting and strain or an extrinsic effect due to defects. The most likely explanation at present is in terms of extrinsic contributions from the mobility of transformation twin walls, as has been described in detail for low frequency anelastic measurements in $LaAlO_3$ and (Ca,Sr)TiO_3 (Harrison and Redfern 2002, Harrison *et al* 2003). A change in twin wall configurations before and after heating into the stability field of the cubic phase would then account for the difference in Q^{-1} during heating and cooling, for example. The degree of attenuation is not as high as has been found at MHz frequencies in $LaAlO_3$ (Carpenter *et al* 2006) or (Ca,Sr)TiO_3 (Walsh *et al* 2008), however.

The $I4/mcm \leftrightarrow Imma$ transition is marked by a significant increase in Q^{-1} although there is some scatter in the data. The scattered values show an overall peak across a relatively wide temperature range (~60 K). This is consistent with some kind of dynamical clustering phenomenon as is proposed to explain the additional elastic softening. Within the $Imma$ stability field, Q^{-1} remains high as if the twin walls are just as mobile as they are in the $I4/mcm$ structure.

The $Imma \leftrightarrow Pnma$ transition is marked by another significant increase in Q^{-1}, presumably reflecting the same classical susceptibility mechanism as occurs at the $Pm\bar{3}m \leftrightarrow I4/mcm$ transition. Q^{-1} then decreases on cooling until ~900 K where it is reduced to similar values as in the cubic phase during heating. The dissipation mechanism operating between ~900 K and the phase transition at 1038 K is not understood, but the decline in Q^{-1} correlates approximately with the increase in K and G. An intrinsic strain/order parameter coupling loss mechanism and/or loss of twin wall mobility could therefore be related to the same geometrical mechanism proposed to account for the reversion of the $Pnma$ structure to a classically stiff (and high-Q) material.

6.3. Comparison with $SrSnO_3$

The transformation behaviour of $SrZrO_3$ appears to be closely analogous to that of $SrSnO_3$, in having exactly the same sequence of structures with increasing temperature (Mountstevens *et al* 2005, Glerup *et al* 2005, Goodwin *et al* 2007). Furthermore, the $Pm\bar{3}m \leftrightarrow I4/mcm$ and $Imma \leftrightarrow Pnma$ transitions in $SrSnO_3$ are also both close to being tricritical in character. A suggestion that the $Imma \leftrightarrow Pnma$ transition involves some significant component of order/disorder (Mountstevens *et al* 2005) was discounted by Goodwin *et al* (2007) and the dominant mechanism is octahedral tilting. The transition temperatures are reduced by substitution of Sr by Ba, allowing the elastic and anelastic anomalies associated with phase transitions in ceramic samples of $Sr_{0.8}Ba_{0.2}SnO_3$ and $Sr_{0.6}Ba_{0.4}SnO_3$ to be investigated by dynamical mechanical analysis at 1–6 Hz (Daraktchiev *et al* 2006, 2007). In $Sr_{0.6}Ba_{0.4}SnO_3$, the $Pm\bar{3}m \leftrightarrow I4/mcm$ transition is marked by a decrease in G and an increase in Q^{-1}. The $I4/mcm \leftrightarrow Imma$ transition is marked by a minimum in G and a maximum in Q^{-1}, which is similar to the variations observed here for $SrZrO_3$ at ~400 kHz. According to the phase diagram given in figure 1 of Daraktchiev *et al* (2007), $Sr_{0.8}Ba_{0.2}SnO_3$ should have the $Pnma$ structure at room temperature. Distinct anomalies in the elastic properties occurring at ~580 and ~850 °C do not match up with the expected phase transitions at ~450 and ~700 °C, however, and the stability limit of the $Pnma$ structure in this sample remains

unclear. Given this ambiguity in the results of Daraktchiev *et al* (2006, 2007), it is not yet possible to conclude that the *Pnma* structure necessarily causes any acoustic dissipation which might be attributed to mobile twin walls. On the other hand, it appears that the elastic and anelastic consequences of the $I4/mcm \leftrightarrow Imma$ transition are rather similar $Sr_{0.8}Ba_{0.2}SnO_3$ at ~1 Hz and in $SrZrO_3$ at ~400 kHz, though the magnitude of the peak in Q^{-1} is smaller at high frequencies than it is at low frequencies. Strikingly similar variations in G and Q^{-1} are observed in the $P4mm \leftrightarrow Amm2$ and $Amm2 \leftrightarrow R3m$ transitions in $BaTiO_3$ (Cheng *et al* 1994, Zhang *et al* 1994), in which the driving mechanism depends on ferroelectric displacements.

The implication is that softening of the shear modulus, G, as the transition point is approached from above and below is a general and characteristic feature of first order phase transitions which are associated with different combinations of order parameter components due to a single instability, irrespective of whether the driving mechanism involves octahedral tilts or ferroelectric displacements. Since this softening is not anticipated on the basis of Landau theory, the likelihood is that it is due to additional fluctuations or clustering when the excess energy due to one tilt/displacement direction becomes the same as the excess energy for a different direction.

7. Conclusion

The hierarchy of ferroelectric transitions analysed by Devonshire (1949, 1951, 1954) for $BaTiO_3$ is not completely reproduced as an analogous tilting sequence in $SrZrO_3$ but the cubic ↔ tetragonal ↔ orthorhombic part of the sequence is essentially the same for both systems. Devonshire showed that the orthorhombic phase can only have an equilibrium stability field if the fourth order Landau coefficient is negative, giving first order transitions (see also Darlington 1997). In $SrZrO_3$ the transitions are close to tricritical (combined fourth order coefficients ≈0 in equation (12)), but there is evidence that the coupling coefficient, λ_5, is not constant. There is some scope for small variations in strain/order parameter coupling causing stabilization of the *Imma* structure relative to $I4/mcm$ or $R\bar{3}c$, therefore. Such effects could also then stabilize *Pnma* ($\approx Imma + P4/mbm$) structures relative to *Cmcm* ($\approx I4/mcm + P4/mbm$).

In this study we have shown, further, that the pattern of elastic properties of $SrZrO_3$ is also closely similar to the pattern previously found for $BaTiO_3$. Order parameter and strain evolution in transformation hierarchies for ferroelectric displacement and ferroelastic tilt systems thus appear to conform to essentially the same mean field model, together with specific deviations from this in the vicinity of each transition. The *Pnma* phase, however, is quite different. The strain variation still shows strain/order parameter coupling, but this is no longer detected in the elastic responses. It thus appears that a combination of R- and M-point tilting causes a suppression of the dynamic relaxation, both in relation to elastic constants and to dissipation by twin walls. This may be a general feature of multiple order parameter phenomena.

Acknowledgments

REAM was supported by a studentship from the Engineering and Physical Sciences Research Council (grant no. EPSRC DTG05 10026782). The RUS equipment was built with a grant from the National Environmental Research Council of Great Britain (grant no. NER/A/S/2000/01055), which is gratefully acknowledged. Thanks also go to Stephen Siklos for guidance with respect to inverse matrices. CJH and MAC acknowledge the support of the Leverhulme Trust, in the form of a Visiting Professorship for CJH. The work is also currently supported by the Australian Research Council, (grant no. DP0877695).

References

Adams D J and Oganov A R 2006 *Phys. Rev.* B **73** 184106
Aleksandrov K S 1976 *Ferroelectrics* **14** 801–5
Aleksandrov K S 1978 *Ferroelectrics* **20** 61–7
Caracas R, Wentzcovitch R, Price G D and Brodholt J 2005 *Geophys. Res. Lett.* **32** L06306
Carlsson L 1967 *Acta Crystallogr.* **23** 901–5
Carpenter M A 2006 *Am. Mineral.* **91** 229–246
Carpenter M A 2007 *Am. Mineral.* **92** 309–27
Carpenter M A, Becerro A I and Seifert F 2001 *Am. Mineral.* **86** 348–63
Carpenter M A, Howard C J, Knight K S and Zhang Z 2006 *J. Phys.: Condens. Matter* **18** 10725–49
Carpenter M A, Li B and Liebermann R C 2007 *Am. Mineral.* **92** 344–55
Carpenter M A, Meyer H-W, Sondergeld P, Marion S and Knight K S 2003 *Am. Mineral.* **88** 534–46
Carpenter M A and Salje E K H 1998 *Eur. J. Mineral.* **10** 693–812
Cheng B L, Gabbay M, Fantozzi G and Duffy W Jr 1994 *J. Alloys Compounds* **211/212** 352–5
Daraktchiev M, Harrison R J, Mountstevens E H and Redfern S A T 2006 *Mater. Sci. Eng.* A **442** 199–203
Daraktchiev M, Salje E K H, Lee W T and Redfern S A T 2007 *Phys. Rev.* B **75** 134102
Darlington C N W 1997 *Phys. Status Solidi* b **203** 73–8
De Ligny D and Richet P 1996 *Phys. Rev.* B **53** 3013–22
Devonshire A F 1949 *Phil. Mag.* **40** 1040–67
Devonshire A F 1951 *Phil. Mag.* **42** 1065–79
Devonshire A F 1954 *Adv. Phys.* **3** 85–130
Fiquet G, Andrault D, Dewaele A, Charpin T, Kunz M and Haüsermann D 1998 *Phys. Earth Planet. Inter.* **105** 21–31
Fossheim K and Fossum J O 1984 Multicritical phenomena *NATO ASI Series* B **106** 113–28
Fossheim K, Martinsen D and Linz A 1974 Anharmonic lattices, structural transitions and melting *NATO ASI Appl. Sci.* **1** 141–6
Fujimori H, Kakihana M, Ioku K, Goto S and Yoshimura M 2004 *J. Ceram. Soc. Japan* **112** 189–92
Glazer A M 1972 *Acta Crystallogr.* B **28** 3384–92
Glazer A M 1975 *Acta Crystallogr.* A **31** 756–62
Glerup M, Knight K S and Poulsen F W 2005 *Mater. Res. Bull.* **40** 507–20
Goodenough J N 1998 *Annu. Rev. Mater. Sci* **28** 1–27
Goodwin A L, Redfern S A T, Dove M T, Keen D A and Tucker M G 2007 *Phys. Rev.* B **76** 174114
Howard C J, Knight K S, Kennedy B J and Kisi E H 2000 *J. Phys.: Condens. Matter* **12** L677–83
Howard C J and Stokes H T 1998 *Acta Crystallogr.* B **54** 782–9
Harrison R J and Redfern S A T 2002 *Phys. Earth Planet. Inter.* **134** 253–72

Harrison R J, Redfern S A T and Street J 2003 *Am. Mineral.* **88** 574–82
Jung D Y and Oganov A R 2005 *Phys. Chem. Mineral.* **32** 146–53
Kennedy B J, Howard C J and Chakoumakos B C 1999 *Phys. Rev.* B **59** 4023–7
Kityk A V, Schranz W, Sondergeld P, Havlik D, Salje E K H and Scott J F 2000 *Phys. Rev.* B **61** 946–56
Kurashina T, Hirose K, Ono S, Sata N and Ohishi Y 2004 *Phys. Earth Planet. Inter.* **145** 67–74
Ledbetter H, Lei M, Hermann A and Sheng Z 1994 *Physica* C **225** 397–403
Li L, Weidner D J, Brodholt J, Alfè D, Price G D, Caracas R and Wentzcovitch R 2006a *Phys. Earth Planet. Inter.* **155** 249–59
Li L, Weidner D J, Brodholt J, Alfè D, Price G D, Caracas R and Wentzcovitch R 2006b *Phys. Earth Planet. Inter.* **155** 260–8
Lufaso M W and Woodward P M 2004 *Acta Crystallogr.* B **60** 10–20
Lüthi B and Rehwald W 1981 Ultrasonic studies near structural phase transitions *Structural Phase Transitions I* (*Springer Topics in Current Physics* vol 23) ed K A Muller and H Thomas (Berlin: Springer) pp 131–84
Matsuda T, Yamanaka S, Kurosaki K and Kobayashi S-I 2003 *J. Alloys Compounds* **351** 43–6
McKnight R E A, Carpenter M A, Darling T W, Buckley A and Taylor P A 2007 *Am. Mineral.* **92** 1665–72
McKnight R E A, Moxon T, Buckley A, Taylor P A, Darling T W and Carpenter M A 2008 *J. Phys.: Condens. Matter* **20** 075229
McKnight R E A, Kennedy B J, Zhou Q and Carpenter M A 2009 *J. Phys.: Condens. Matter* **21** 015902
Megaw H D 1973 *Crystal Structures: A Working Approach* (Philadelphia, PA: Saunders) pp 285–302
Meyer H-W, Carpenter M A, Graeme-Barber A, Sondergeld P and Schranz W 2000 *Eur. J. Mineral.* **12** 1139–50
Meyer H-W, Marion S, Sondergeld P, Carpenter M A, Knight K S, Redfern S A T and Dove M T 2001 *Am. Mineral.* **86** 566–77
Migliori A and Sarrao J L 1997 *Resonant Ultrasound Spectroscopy: Applications to Physics, Material Measurements and Nondestructive Evaluation* (New York: Wiley)
Mountstevens E H, Redfern S A T and Attfield J P 2005 *Phys. Rev.* B **71** 220102
Ono S, Kikegawa T and Iizuka T 2004a *Phys. Earth Planet. Inter.* **145** 9–17
Ono S, Ohishi Y and Mibe K 2004b *Am. Mineral.* **89** 1480–5
Rehwald W 1973 *Adv. Phys.* **22** 721–55
Salje E K H 1989 *Phil. Trans. R. Soc.* A **328** 409–16
Salje E K H, Wruck B and Thomas H 1991 *Z. Phys.* B **82** 399–404
Schaller R, Fantozzi G and Gremaud G (ed) 2001 *Mechanical Spectroscopy Q^{-1} 2001: With Applications to Materials Science* (Zurich: Trans Tech Publications) pp 364–5
Schranz W, Sondergeld P, Kityk A V and Salje E K H 1999 *Phase Transit.* **69** 61–76
Schreuer J and Thybaut C 2005 *Proc. IEEE Ultrasonics Symp. 2005* pp 695–8
Schreuer J, Thybaut C, Prestat M, Stade J and Haussühl S 2003 *Proc. IEEE Ultrasonics Symp. (2003)* pp 196–9
Slonczewski J C and Thomas H 1970 *Phys. Rev.* B **1** 3599–608
Sondergeld P, Schranz W, Kityk A V, Carpenter M A and Libowitzky E 2000 *Phase Transit.* **71** 189–203
Stixrude L and Cohen R E 1993 *Nature* **364** 613–15
Walsh J W, Taylor P A, Buckley A, Darling T W, Schreuer J and Carpenter M A 2008 *Phys. Earth Planet. Inter.* **167** 110–7
Watt J P 1979 *Appl. Phys.* A **50** 6290–5
Watt J P and Peselnik L 1980 *J. Appl. Phys.* A **51** 1525–31
Wentzcovitch R M, Martins J L and Price G D 1993 *Phys. Rev. Lett.* **70** 3947–50
Zhang J X, Zheng W, Fung P C W and Liang K F 1994 *J. Alloys Compounds* **211/212** 378–80